Heave Motion Estimation from IMU measurements in Hybrid Aerial-Amphibious Drones and Horizontal Take-Off Window Prediction

Andrea Capuozzo, Fabio Ruggiero, Vincenzo Lippiello

***Abstract*— Employing hybrid aerial-amphibious drones, for activities in the marine environment, comes with a series of challenges that concern managing the interaction between the robot and the water surfaces, especially in the presence of waves. This paper focuses on the take-off transition from water to air, aiming to identify and predict those time windows in which the drone has a close to zero roll and pitch (horizontal attitude) and the propellers are the furthest from the water surface, thus optimizing the take-off. The proposed solution merges the measurement of the drone vertical displacement, due to the wavefronts, with the attitude data, returning a prediction signal that marks the best take-off windows in the immediate future. The idea has been validated through numerous simulated case studies.**

I. INTRODUCTION

Hybrid aerial-amphibious drones, or unmanned aerial-aquatic vehicles (UAAVs), are versatile robotic systems capable of operating in both air and water, typically within a fully integrated structure. These vehicles are increasingly gaining attention for their potential to simplify and enhance technical operations at sea [1], [2].

In marine biology, tasks such as mapping, monitoring, and sampling aquatic environments are essential for research. Currently, these activities are primarily performed by trained scuba divers, requiring significant resources (e.g., fuel, boat maintenance, and scuba equipment) while posing risks to both human operators and marine ecosystems (e.g., water and noise pollution). Equipped with specialized tools, UAAVs deployed from the mainland can autonomously reach sites of interest, executing these tasks with zero human risk, reduced environmental impact, and improved cost efficiency. Additionally, UAAVs can expedite marine inspection operations around offshore sites by being launched directly from them, eliminating the need for specialized personnel or equipment.

Despite the advantages offered by this technology, several challenges must be addressed, particularly concerning the transition between air and water, which becomes increasingly complex in non-calm sea conditions. This paper focuses on the take-off transition in the presence of waves, where oscillatory motion affects the UAAV's attitude. If the take-off command is issued at an arbitrary moment, the UAAV may attempt take-off from a non-horizontal orientation (i.e., when its attitude is not parallel to the water surface). This misalignment can cause water contact with one or more propellers, slowing them down or leading to mechanical failures that jeopardize the operation. In the worst-case scenario, this could result in a capsize.

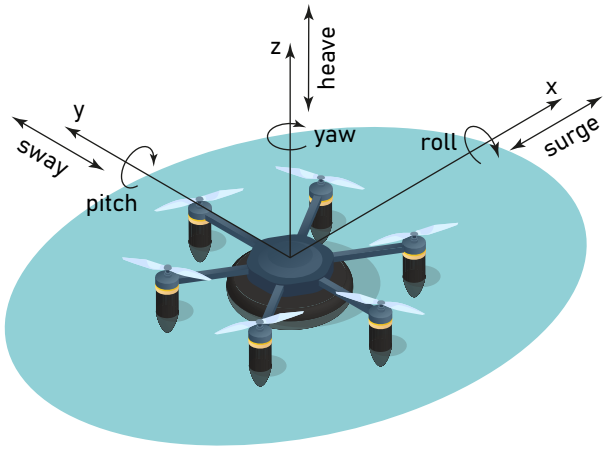

Fig. 1: Diagram showing the six degrees of freedom of an UAAV floating body.

This work explores a method to ensure that the take-off command for an UAAV is issued only when its attitude is nearly horizontal (i.e., with roll and pitch angles close to zero) and when the propellers are maximally distanced from the water surface. Empirical observations indicate that these conditions are best met when the UAAV is at the crest of a wave rather than in a trough between two wavefronts. To execute take-off at the optimal moment, it is crucial to anticipate sea conditions in advance. Specifically, the UAAV's position relative to the wavefronts and its attitude in the immediate future must be predicted. Notably, determining when the drone is at the crest does not require a full estimation of wave parameters. Instead, it suffices to measure the vertical displacement, or heave motion (see Fig. 1), of the floating body using acceleration data from a single onboard inertial measurement unit (IMU). This approach is valid because the UAAV's compact size prevents its submerged hull from acting as a low-pass filter for wave-induced motion [3], making the ship-as-a-wave-buoy analogy applicable. As a result, the difference between the wave height at the drone's center of mass and its altitude above sea level is negligible. Once heave motion, roll, and pitch data are recorded over a time interval, a fast Fourier transform (FFT) is applied to

The research leading to these results has been supported by *Centro Nazionale 5* (CN5) - *National Biodiversity Future Center* (NBFC) - *SPOKE 1* (Codice progetto MUR: CN0000033 CUP UNINA: E63C22000990007). The authors are solely responsible for its content.

The authors are with the PRISMA Lab, Department of Electrical Engineering and Information Technology, University of Naples Federico II, Via Claudio 21, Naples, 80125, Italy. Corresponding author's email: andrea.capuozzo@unina.it

predict the UAAV's position relative to wave crests and the instances when it achieves a level attitude. These predictions are then combined to determine the best future take-off windows. With this information, the flight controller can calculate the optimal moment to issue the take-off command, ensuring that rotor transients align with the most favorable conditions for a successful water detachment.

The paper outline is organized as follows. Section II provides the state of the art dealing with the UAAVs water take-off and IMU sensors usage. Section III contains the necessary assumptions and all the mathematical steps to predict the take-off windows. Section IV illustrates the results obtained in different simulated scenarios, while Section V goes deeply in discussing the results. Finally, Section VI draws the conclusions and outlines potential future developments.

II. STATE OF THE ART

The challenge of managing water-to-air transitions for amphibious UAAVs has been addressed in the literature through various approaches. In [4], fixed-wing amphibious drones with tilting propellers are proposed for take-off from calm lake conditions. A morphing structure for underwater take-off is explored in [5], though adverse sea conditions are not considered. In [6], an UAAV prototype equipped for underwater sampling and inspection, similar to the reference model used in this work, is introduced, highlighting the challenges of achieving a safe takeoff from water in wave conditions ranging from $0.10-0.50$ m. Rough sea conditions are primarily discussed in relation to landing on oscillating platforms, such as ship decks, as examined in [7].

IMU sensors are commonly used for sea wave measurement and monitoring. Various methods integrating IMUs with other technologies to enhance measurement accuracy are discussed in [8], [9]. Specifically, in [10], a method for estimating wave height and period using a single low-precision IMU sensor is presented, forming the basis for the heave motion measurement approach adopted in this paper.

A. Contributions

To the best of the authors' knowledge, the problem of managing take-off in the presence of sea waves has not yet been addressed in the literature. This work contributes by (i) applying state-of-the-art methods to estimate, from a single IMU sensor, the UAAV vertical displacement due to wave motion; (ii) identifying the time windows in which the UAAV's attitude remains approximately horizontal and utilizes a brief recording of IMU and attitude data to predict the UAAV's position relative to wave crests and determine future time windows where its attitude remains leveled; and (iii) combining these predictions, the proposed approach provides the flight controller with optimal take-off windows, minimizing the risks associated with water-propeller interaction.

III. METHODOLOGY

Before discussing the mathematical details of how estimations and predictions are obtained, it is necessary to state some preliminary assumptions.

Fig. 2: PLaCE UAAV.

A. Wave modeling

The wave field at the surface sea level is modeled as a summation of Gersnter waves [11]. Since take-off occurs over a short time window, the stochastic nature of the sea and uncertainties due to external factors can be reasonably neglected and the sea state considered stationary. Define a world inertial frame Σ_w. Let P be a point on the sea surface, whose components in Σ_w are $x, y, z \in \mathbb{R}$. Define $\mathbf{x} = \begin{bmatrix} x & y \end{bmatrix}^T \in \mathbb{R}^2$ as the horizontal components of P. When undisturbed, the coordinates of P are denoted as $\mathbf{x}_0$ and $z_0 = 0$. When the waves pass by, the displacement of P is

$$\begin{aligned} \mathbf{x} =& \mathbf{x}_0 - \sum_{i=1}^{N_w} \frac{\mathbf{k}_i}{k_i} A_i \sin(\mathbf{k}_i^T \mathbf{x}_0 - \omega_i t + \phi_i), \\ z =& \sum_{i=1}^{N_w} A_i \cos(\mathbf{k}_i^T \mathbf{x}_0 - \omega_i t + \phi_i), \end{aligned} \tag{1}$$

where $t \in \mathbb{R}$ is the time variable, $N_w \in \mathbb{N}_0$ is the number of component waves. For each one of them, $A_i > 0$ is the amplitude, $\mathbf{k}_i \in \mathbb{R}^2$ is the wavevector, that is the horizontal vector pointing the wave travel direction, with $\|\mathbf{k}_i\| = k_i$, $\omega_i > 0$ is the angular frequency, $\phi_i \in \mathbb{R}$ is the wave phase, and kA_i determines the steepness of the component wave. The wavevector $\mathbf{k}_i$ is correlated to the wavenumber through the following relation $k_i = 2\pi/\lambda_i$, with $\lambda_i > 0$ the wavelength. The angular frequency and the wavenumber are related through the deep water dispersion relation [12], $\omega_i^2 = g k_i$, where $g > 0$ is the gravity acceleration. The properties of the wave components are derived from the Pierson-Moskowitz spectrum sampling [13].

B. UAAV specification

The UAAV considered in this study is the PLaCE drone [14], shown in Fig. 2, an amphibious hexacopter with circular symmetry designed for both aerial sea surface surveys and underwater environmental measurements, achieved by landing on water and deploying the required sensors. The main buoyant disk is located beneath the central body, with six additional buoyant structures—one under each propeller—for enhanced stability.

C. Problem statement

Consider a UAAV that must take off from the water surface in the presence of sea waves, which could potentially jeopardize the water-air transition. Using onboard IMU data, attitude measurements, and propellers transient dynamics, the objective is to predict and identify future safe take-off time windows, ensuring that the drone maintains a horizontal attitude and avoids wave impact during the transition.

D. Heave measurement

Define a body frame Σ_b attached to the UAAV and a reference frame Σ_r, which shares the same origin as Σ_b but has its axes always aligned with those of Σ_w. As stated in [10], to utilize the IMU data the measured acceleration must be expressed in Σ_r. Defining $\gamma, \theta, \varphi \in \mathbb{R}$ as the roll, pitch, and yaw angles, respectively, representing the attitude of Σ_b in Σ_w and Σ_r, the IMU acceleration $\mathbf{a}_b \in \mathbb{R}^3$ in Σ_b can be expressed in Σ_r through $\mathbf{a}_r \in \mathbb{R}^3$ as

$$\mathbf{a}_r = \begin{bmatrix} c\theta c\varphi & s\gamma s\theta c\varphi - c\gamma s\varphi & c\gamma s\theta c\varphi + s\gamma s\varphi \\ c\theta s\varphi & s\gamma s\theta s\varphi + c\gamma s\varphi & c\gamma s\theta s\varphi - s\gamma c\varphi \\ -s\theta & s\gamma c\theta & c\gamma c\theta \end{bmatrix} \mathbf{a}_b, \quad (2)$$

where $cx = \cos x$ and $sx = \sin x$.

To compute the UAAV heave motion, the third component of $\mathbf{a}_r$ is of interest and it is denoted as $a_z \in \mathbb{R}$. To isolate the wave perturbation effect from gravity, a_z must be modified as

$$\bar{a}_z = -\sin\theta a_{0,x} + \sin\gamma\cos\theta a_{0,y} + \cos\gamma\sin\theta a_{0,z} - g. \quad (3)$$

To compute the heave motion, that is the displacement along the vertical axis of Σ_r, it is necessary to integrate twice the acceleration signal. However, its integration with classic numerical methods would lead to error accumulation. To avoid this issue, the process will be done in the frequency domain using the FFT. Since the signal is sampled, the discrete Fourier transform (DFT) algorithm will be applied [15]

$$\bar{A}_z(k) = \sum_{n=0}^{N-1} \bar{a}_z(n) e^{-j2\pi kn/N}, \quad (4)$$

where $\bar{A}_z(k)$ denotes the entire DFT, $N \in \mathbb{N}_0$ is the number of points sampled in the time interval $T > 0$, $k \leq N-1$, and $n \leq N-1$. Before proceeding to integration, note that it is not necessary to consider the 0 Hz component of $\bar{A}_z$: experimentally, it is possible to verify that $\bar{a}_z$ has a negligible mean value, thus the 0 Hz component can be ignored in the transformed signal. The heave motion can now be expressed in the frequency domain as [10]

$$H(k) = \frac{\bar{A}_z(k)}{(j2\pi f_k)^2}, \ \forall k \mid f_k \neq 0, \quad (5)$$

where $f_k > 0$ is the frequency associated to the k-th harmonic component, j is the imaginary unit. By computing the inverse discrete Fourier transform (IDFT), the heave motion signal $h(t_n)$, over the time interval T and with t_n as the n-th time sample, is successfully retrieved.

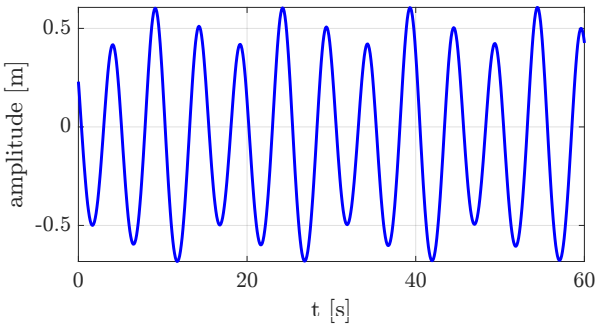

Fig. 3: Example of UAAV heave motion.

E. Identifying flat attitude windows

To deal with the prediction of the take-off windows, it is required to identify the intervals of time, in which the UAAV has a horizontal configuration, that is when $|\gamma| < \varepsilon$ and $|\theta| < \varepsilon$, with $\varepsilon > 0$ as given tolerance representing the boundaries in which it is considered horizontal. From the horizontal configuration condition, the following square wave signal is obtained

$$fa(t_n) = \begin{cases} 1 & \text{if} \quad |\gamma(t_n)| < \varepsilon \wedge |\theta(t_n)| < \varepsilon, \\ 0 & \text{otherwise.} \end{cases} \quad (6)$$

This signal has its high value when the drone is in the boundaries of its horizontal attitude, zero otherwise. Further processing of $fa(t_n)$ is required to ensure that, when the UAAV achieves the desired attitude, the distance between the propellers and the water surface is maximized. As stated in Section I, this condition occurs when the UAAV is at the wave crest, where the heave reaches its maximum value, indicating the drone has undergone its maximum vertical displacement. Running simulations (whose details are given in the next Section) with different wave parameters, it is possible to confirm that the heave maximum is always positive, while the minimum is always negative (see Fig. 3). Hence, a new square wave can be defined as

$$\bar{fa}(t_n) = \begin{cases} 1 & \text{if} \quad fa(t_n) = 1 \wedge h(t_n) > 0, \\ 0 & \text{otherwhise.} \end{cases} \quad (7)$$

F. Prediction of take-off windows

Let T_r be the data recording time frame, $\bar{a}_z(t_r)$ and $fa(t_r)$, with $t_r \in T_r$ the acceleration and square wave, computed in (3) and (6), respectively, and recorded in T_r. Define $T_p > 0$ as the prediction time frame in which the take-off windows must be identified. Suppose that both time frames have equal length and are contiguous in time. The objective is to predict the UAAV heave motion $h_p(t_p)$ and the horizontal attitude $fa_p(t_p)$ in T_p, with $t_p \in T_p$.

Applying the DFT to $\bar{a}_z(t_r)$ and $fa(t_r)$, $\bar{A}_z(k)$ and $FA(k)$ are obtained, respectively, whose magnitudes and phases are given by $|\bar{A}_z(k)|$, $|FA(k)|$, $\angle\bar{A}_z(k)$ and $\angle FA(k)$, respectively. Using these components, the acceleration and

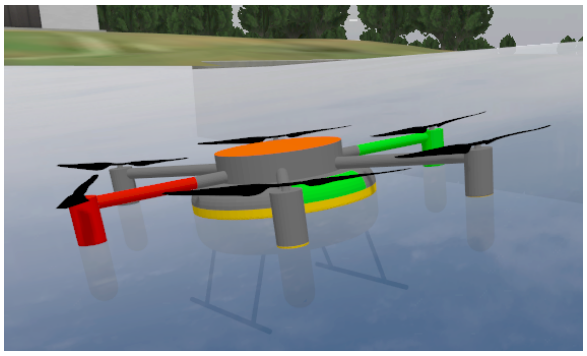

Fig. 4: Example of simulation with PLaCE mockup landed on the water surface.

square wave in T_p can be predicted as

$$\begin{aligned} \bar{a}_{z,p}(t_p) &= \sum_{k=0}^{N-1} \frac{|\bar{A}_z(k)|}{N} \cos(2\pi f_k t_p + \angle \bar{A}_z(k)), \\ fa_p(t_p) &= \sum_{k=0}^{N-1} \frac{|FA(k)|}{N} \cos(2\pi f_k t_p + \angle FA(k)). \end{aligned} \tag{8}$$

Applying (4) and (5) to $\bar{a}_{z,p}(t_p)$, the heave motion $h_p(t_p)$ is retrieved. Finally, combining $h_p(t_n)$ and $fa_p(t_p)$, in the same manner of (7), yields the square wave signal $\bar{fa}_p(t_p)$. This identifies the future time window in which the UAAV maintains a horizontal attitude while being at the wave crests.

As a final step, each identified take-off time window must be assessed for acceptability based on the UAAV rotor's transient. A time window is deemed acceptable if its duration exceeds the time required for the UAAV to fully detach from the water after initiating take-off. It is important to note that the *lift-off* (defined as the moment the UAAV begins its ascent, which occurs only after the propellers have reached the required thrust level) does not coincide with the moment the flight controller issues the *take-off signal*, due to the transient effects of the rotors.

IV. SIMULATIONS

A. Simulation set up

The simulations have been performed on a standard personal computer with an *Intel Core i7* (11^{th} generation) processor and 32 GB of RAM, running *Ubuntu 22.04* as operative system.

The marine environment was simulated using the *Virtual RobotX* (VRX) simulation environment [16] running on *Gazebo Garden v 7.9.0* (see Fig. 4), with modifications applied to account for the shape of the UAAV floating components and the dampening effect in the drone-water interactions [17]. Without the latter, the buoyant force would have behaved like an elastic force, causing the UAAV to exhibit a continuous oscillatory behavior upon contact with the sea surface. The flight dynamic of the UAAV has been simulated using the *PX4 Autopilot* [18] firmware with the software in the loop (SITL) mode. As a simplyfing assumption, UAAV sensors measurements are considered noise-free. *ROS 2 Humble* was used to process and collect all IMU and attitude data, with a 10 Hz sampling frequency. *MATLAB* was used for applying the DFT and prediction algorithm to the recorded data.

In the presented case studies, the attitude threshold was set to $\varepsilon = 4°$. The time windows, T_r and T_p were both set to 20 s, selected through a trial-and-error approach to minimize prediction error. The first prediction is obtained 20 s after the algorithm starts, with subsequent predictions generated at the same time intervals. The minimum duration for a valid take-off window was set to 1.5 s. The VRX simulator models the wave field following the formulation in (1), allowing the user to modify the parameters and include up to three component waves. The following case studies differ based on: wave period T, wave median amplitude A, angular direction of the wavevector d, number of component waves N, angle between component waves α, and the presence of additive white Gaussian noise on IMU measurements. Details are in Table I.

Case study	T	A	d	N	α	noise
Case *1)*	5 s	0.5 m	0.7 rad	2	0.4 rad	no
Case *2)*	10 s	1 m	1.2 rad	2	1.2 rad	no
Case *3)*	3 s	0.2 m	0.7 rad	2	0.6 rad	no
Case *4)*	10 s	2.5 m	1.2 rad	3	0.1 rad	no
Case *5)*	5 s	0.5 m	0.7 rad	2	0.4 rad	yes

TABLE I: Simulation parameters in the different case studies.

B. Case study 1)

In Fig. 5, the heave motion prediction and the corresponding prediction error are shown from 20 s up to 80 s. The prediction algorithm's performance is acceptable, with the largest error occurring at the points of maximum and minimum displacement. However, the heave sign is preserved, ensuring the correct distinction between the flat attitude windows, as described in Sections III-E and III-F. The predicted flat take-off windows are displayed in Fig. 6 along with the associated prediction error, which takes a value of 1 if the predicted window is delayed and -1 if it is early. The green-highlighted windows have a duration of at least 1.5 s and are therefore acceptable for take-off. The prediction exhibits minor delays or anticipations, averaging approximately $0.2 \approx 0.3$ s, which is negligible. These errors stem from both the errors in the square wave prediction and the heave prediction, used in (7) for the final processing. Overall, the prediction performance can be considered acceptable.

C. Case study 2)

In this scenario, the period and median amplitude are doubled compared to the previous case. Figures 7 and 8 illustrate the prediction performance for both heave motion and take-off windows. Throughout this simulation, the attitude of the UAAV always remains within the prescribed boundaries at all times. Consequently, the errors in the predicted take-off windows stem solely from the heave prediction error. Despite larger waves, the prediction performance remains comparable to that of case study *1)*.

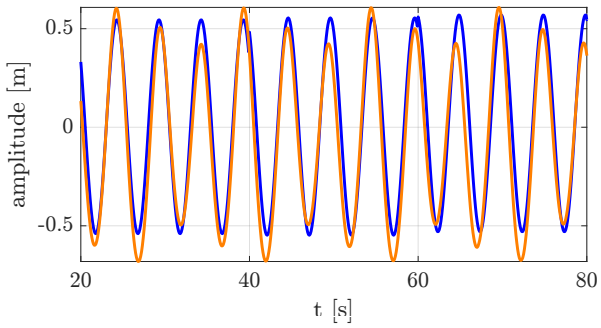

(a) Predicted heave motion (blue) and reference (orange).

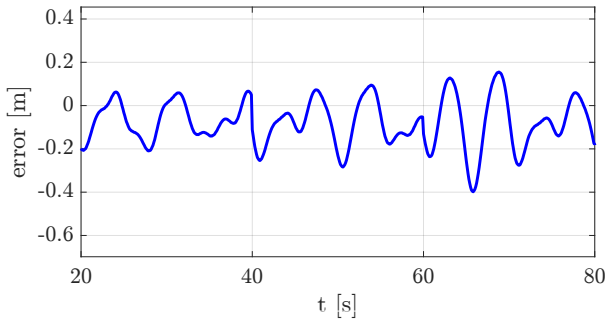

(b) Prediction error.

Fig. 5: Heave motion prediction in case study *1)*.

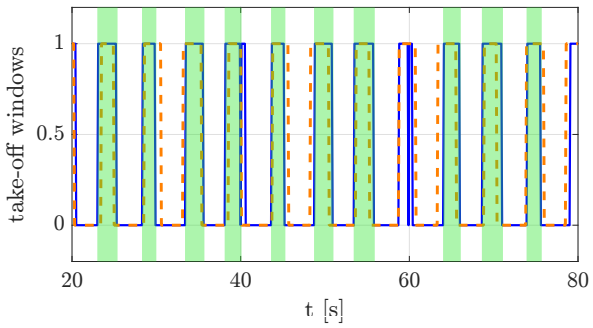

(a) Predicted take-off windows (blue) and reference (dashed orange), highlighted in green the feasible windows.

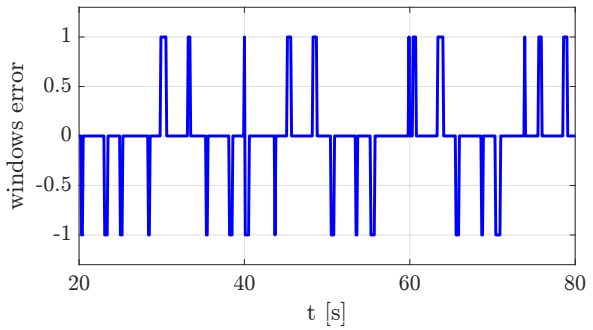

(b) Prediction error.

Fig. 6: Flat take-off window prediction in case study *1)*.

D. Case study 3)

In this simulation, the wave period and amplitude have been reduced, resulting in smaller but faster waves that generate stronger accelerations on the UAAV body. The prediction results and corresponding errors are shown in Fig.s 9 and 10. Under these conditions, it is evident that the algorithm does not perform well. Although some take-off windows are deemed acceptable, they are completely out of phase with the reference and then the take-off is unsuitable.

E. Case study 4)

This case study shares similar parameters with case study *2)*, but includes an additional third component wave. As a result, the UAAV experiences increased perturbations and higher acceleration. However, the time required to traverse a single wave is longer compared to all previous simulations. Figure 11 presents the heave prediction alongside its corresponding error. Despite the presence of the third wave, the prediction performance remains acceptable. As shown in Fig. 12, despite the irregular motion of the UAAV, the only two acceptable take-off windows are identified, both exhibiting a slight anticipation with respect to the reference.

F. Case study 5)

A final case study assesses the impact of additive white Gaussian noise with a signal-to-noise ratio (SNR) of 5 dB on IMU measurements by re-evaluating prediction performance in case study 1). Figures 13 and 14 show the results for this case study. The combined use of FFT with high-frequency filtering and double integration [19] results in only a slight degradation of heave prediction, which is still satisfactory. However, noise in the roll and pitch measurements significantly compromises the square wave computation in (6), causing unreliable threshold detection (see Fig. 14). Although not shown for brevity, provided that no more than two wave components are present, simulations confirm that take-off window detection remains acceptable when the SNR is equal or above 10 dB.

V. DISCUSSION

The results presented in Section IV require a careful analysis of multiple aspects, highlighting both the strengths of the algorithm and potential areas for improvement.

The choice of the recording window duration plays a crucial role in ensuring accurate predictions. In four out of five simulations, the prediction window length is a multiple of the wave period. However, in case study *3)*, where this condition is not met, the prediction performance deteriorates, increasing the risk of an incorrect take-off.

Another critical factor influencing the prediction and integration algorithms is the signal sampling frequency and the number of samples collected within the recording window. These parameters directly affect the Nyquist frequency and the resolution in the frequency domain. The sampling frequency is constrained by the minimum measurement rate of the onboard sensors, in this case, the IMU. Meanwhile, the number of collected samples is also limited by the desired algorithm speed, which directly impacts the lengths of the

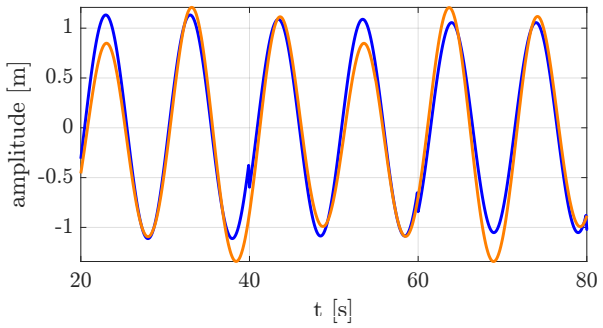

(a) Predicted heave motion (blue) and reference (orange).

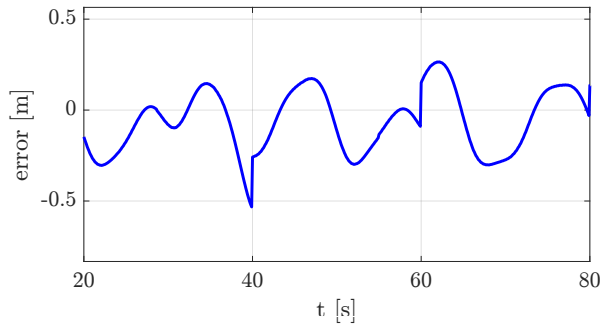

(b) Prediction error.

Fig. 7: Heave motion prediction in case study *2)*.

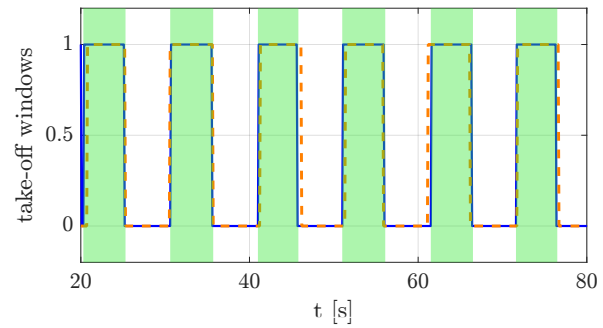

(a) Predicted take-off windows (blue) and reference (dashed orange), highlighted in green the feasible windows.

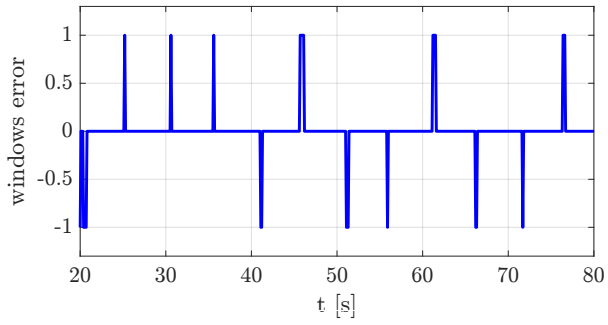

(b) Prediction error.

Fig. 8: Flat take-off window prediction in case study *2)*.

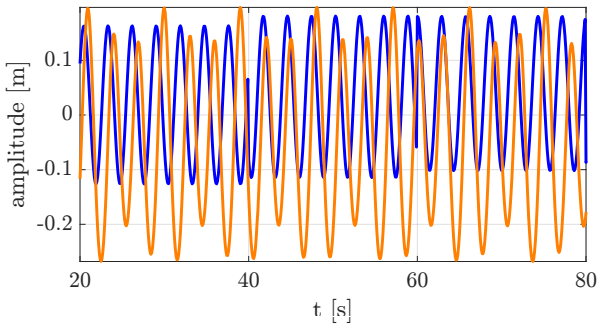

(a) Predicted heave motion (blue) and reference (orange)

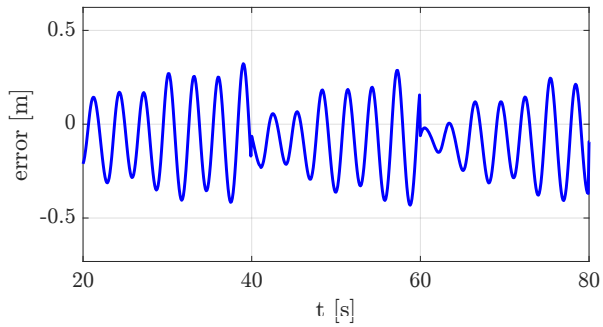

(b) Prediction error

Fig. 9: Heave motion prediction in case study *3)*

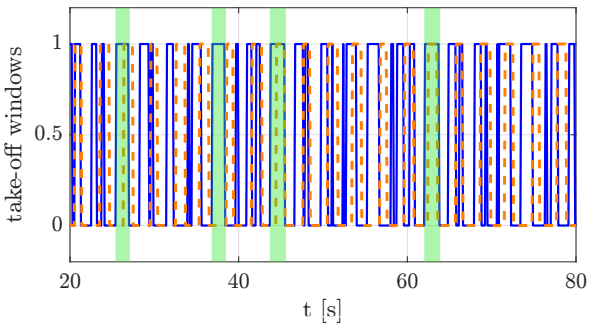

(a) Predicted take-off windows (blue) and reference (dashed orange), highlighted in green the feasible windows.

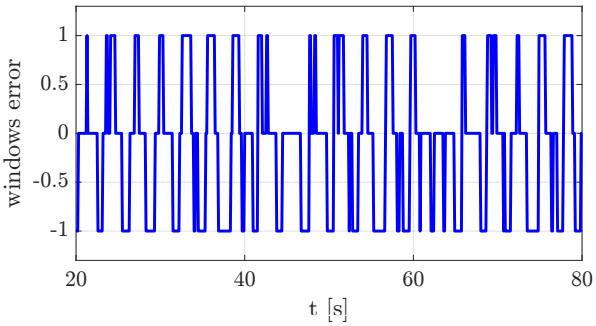

(b) Prediction error

Fig. 10: Flat take-off window prediction in case study *3)*

recording and prediction windows.

Closely related to the sampling frequency and the number of collected samples is the number of harmonic components considered during the prediction and integration processes. Through a trial-and-error approach, it has been verified that for optimal square wave prediction performance, all

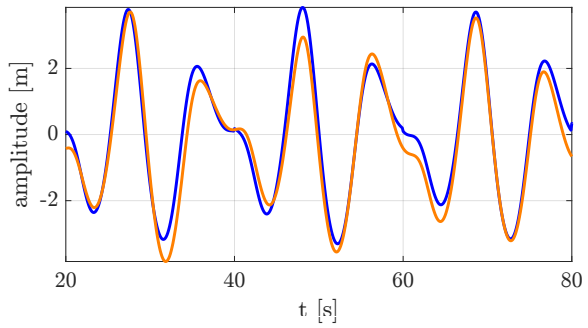

(a) Predicted heave motion (blue) and reference (orange)

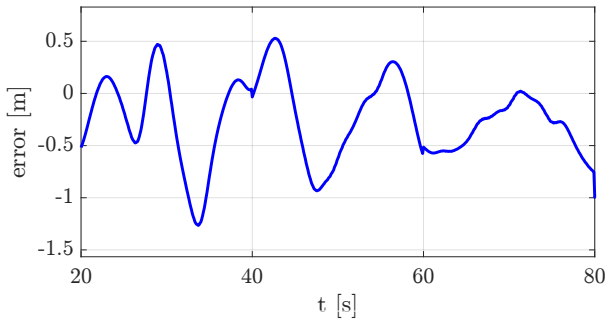

(b) Prediction error

Fig. 11: Heave motion prediction in case study *4)*

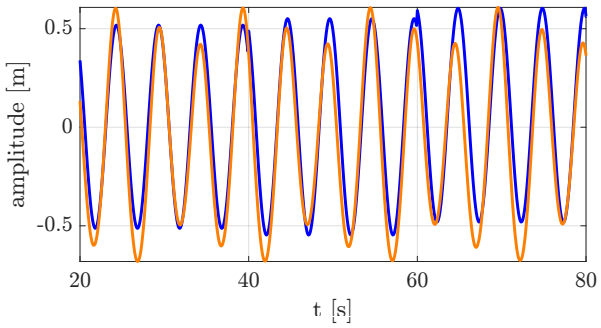

(a) Predicted heave motion (blue) and reference (orange)

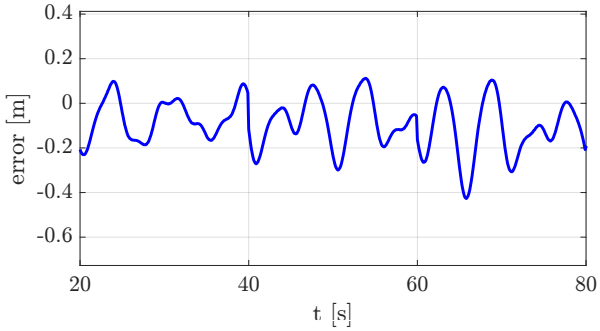

(b) Prediction error

Fig. 13: Heave motion prediction in case study *5)*

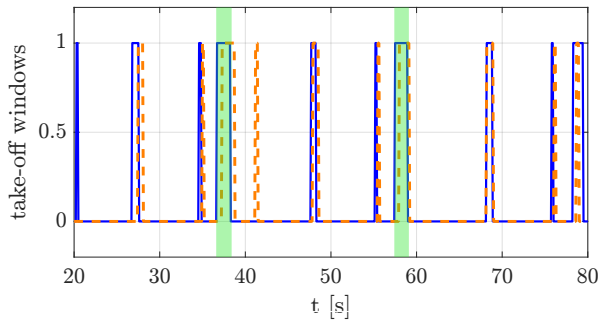

(a) Predicted take-off windows (blue) and reference (dashed orange), highlighted in green the feasible windows.

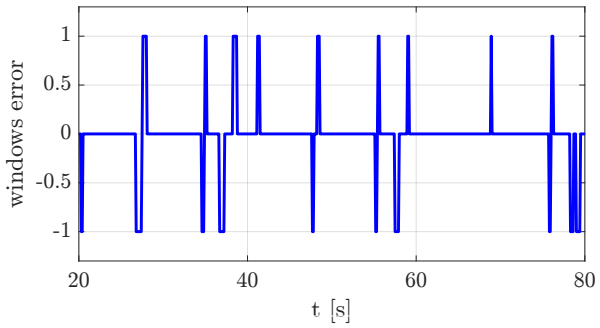

(b) Prediction error

Fig. 12: Flat take-off window prediction in case study *4)*

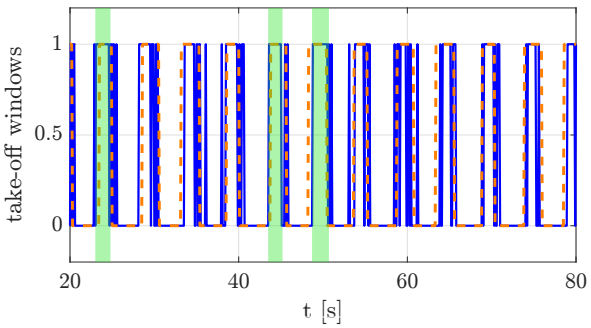

(a) Predicted take-off windows (blue) and reference (dashed orange), highlighted in green the feasible windows.

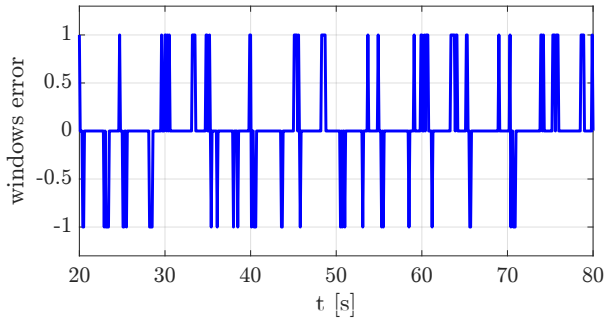

(b) Prediction error

Fig. 14: Flat take-off window prediction in case study *5)*

harmonic components from 0 to $N-1$ must be considered in (8). However, this is not the case for acceleration prediction and integration, where finer tuning is required. In case studies *1)* and *2)*, the best results were obtained by using the first $20 \approx 30$ harmonic components for acceleration prediction within T_p and no more than the first 4 components for the

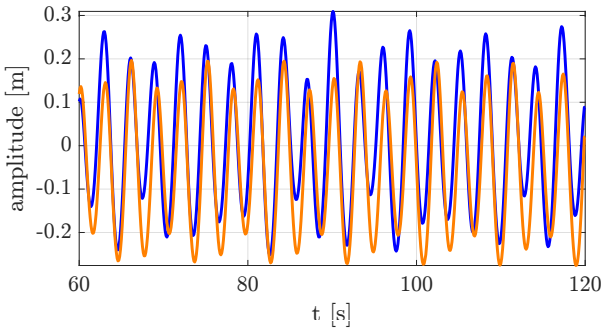

Fig. 15: Predicted heave motion (blue) and reference (orange) in case study *3)* with different parameters.

integration step. In case study *4)*, the number of components used for prediction was increased to 50, while the integration step utilized up to 10 components. Exceeding these limits during integration, without increasing the number of samples, significantly worsens performance. Figure 15 illustrates the heave motion prediction results for case study *3)*, with $T_r = T_p = 60$ s, considering the first 50 harmonics for prediction and up to 20 harmonics for integration. The performance shows significant improvement. Although omitted for brevity, it can be easily demonstrated that increasing the recording window to a thousand samples further enhances the performance of case study *3)*.

Another key factor in performance analysis is the relationship between wavelength, wave period, and the acceleration acting on the UAAV. The case studies show that prediction accuracy decreases with stronger external forces, but improves when the wave period—and thus wavelength—increases, as the UAAV traverses waves more smoothly, reducing dynamic disturbances.

Lastly, in the presence of noise on IMU measurements, while the heave prediction still demonstrates promising performance, it is advisable to robustify the approach used for square wave prediction (see next section for possible ways of improvement).

VI. CONCLUSION AND FUTURE WORK

This paper proposes a new approach to the water-air transition during UAAV take-off in presence of sea waves. The primary objective is to ensure a safe detachment from the water surface avoiding wave impact on the propellers, that could slow them down or cause malfunctions or, in the worst-case scenario, capsizing the drone. The proposed solution consists of an FFT-based algorithm that predicts, in the immediate future, the UAAV position and attitude relative to the wave field, enabling optimized take-off timing. Simulations confirmed the goodness of this new approach.

This work can be further extended by accelerating the prediction process by reducing the time window duration, developing an auto-tuning method for the prediction and integration parameters, and explicitly addressing the presence of noise on IMU measurements. The robustness of the square wave prediction could be improved by exploring alternative computation methods for (6), such as directly predicting the roll and pitch signals before calculating the attitude-based square wave. Ultimately, this study establishes a foundation for future advancements in marine operations involving hybrid aerial-amphibious drones.

REFERENCES

[1] A. P. Colefax, P. A. Butcher, B. P. Kelaher, "The potential for unmanned aerial vehicles (UAVs) to conduct marine fauna surveys in place of manned aircraft", *ICES Journal of Marine Science*, vol. 75, n. 1, 2018, pp. 1—8.

[2] S. Yuan, Y. Li, F. Bao, H. Xu, Y. Yang, Q. Yan, S. Zhong, H. Yin, J. Xu, Z. Huang, J. Lin, "Marine environmental monitoring with unmanned vehicle platforms: Present applications and future prospects", *Science of The Total Environment*, vol. 858, part 1, 2023.

[3] U. D. Nielsen, H. B. Bingham, A. H. Brodtkorb, T. Iseki, J. J. Jensen, M. Mittendorf, R. E. G. Mounet, Y. Shao, G. Storhaug, A. J. Sørensen, T. Takami, "Estimating waves via measured ship responses", *Scientific Reports*, vol. 13, 2023.

[4] E. Tétreault, D. Rancourt, A. L. Desbiens, "Active Vertical Takeoff of an Aquatic UAV", *IEEE Robotics and Automation Letters*, vol. 5, n. 3, 2020, pp. 4844–4851.

[5] J. Hu, B. Xu, J. Feng, D. Qi, J. Yang, C. Wang, "Research on water-exit and take-off process for Morphing Unmanned Submersible Aerial Vehicle", *China Ocean Engineering*, vol. 31, 2017, pp. 202–209.

[6] A. T. Farinha, J. di Tria, M. Reyes, C. Rosas, O. Pang, R. Zufferey, F. Pomati, M. Kovac, "Off-shore and underwater sampling of aquatic environments with the aerial-aquatic drone MEDUSA", *Frontiers in Environmental Science*, vol. 10, 2022.

[7] J. R. Hervas, M. Reyhanoglu, H. Tang, "Automatic landing control of Unmanned Aerial Vehicles on moving platforms," *2014 IEEE 23rd International Symposium on Industrial Electronics*, 2014, pp. 69–74.

[8] J. T. Ølberg, P. Bohlinger, Ø. Breivik, K. H. Christensen, B. R. Furevik, L. R. Hole, G. Hope, A. Jensen, F. Knoblauch, N. Nguyen, J. Rabault, "Wave measurements using open source ship mounted ultrasonic altimeter and motion correction system during the one ocean circumnavigation", *Ocean Engineering*, vol. 292, 2024.

[9] Y. Huang, C. Kuo, C. Shih, L. Lin, K. Chiang, K. Cheng, "Monitoring High-frequency Ocean signals using low-cost GNSS/IMU buoys", *The International Archives of the Photogrammetry, Remote Sensing and Spatial Information Sciences*, vol. 41, 2016.

[10] Y. Zhang, L. Qi, J. Dong, Q. Wen, M. Lv, "Data Processing Based on Low-Precision IMU Equipment to Predict Wave Height and Wave Period", *2019 2nd International Conference on Data Intelligence and Security*, 2019, pp. 103–107.

[11] J. Tessendorf, "Simulating Ocean Water", *Simulating nature: realistic and interactive techniques*, vol. 1, 2001.

[12] R. G. Dean, R. A. Dalrymple, "Water wave mechanics for engineers and scientists", vol. 2, *World Scientific Publishing Company*, 1991.

[13] S. Thon, J. M. Dischler, D. Ghazanfarpour, "Ocean waves synthesis using a spectrum-based turbulence function", *Proceedings Computer Graphics International*, 2000.

[14] L. Miozza, R.Schiavon, T. Grasso, J. Cacace, G. Paduano, F. Pierro, V. Lippiello, D. Speranza, A. Giuggioli, A. Vignali, A. Dell'Anno, "An Amphibious Drone for Aerial, Surface, and Underwater Assets and Environmental Remote Monitoring To Support the Sustainability of Unmanned Offshore Converted Platform", *OMC Med Energy Conference and Exhibition*, 2023.

[15] M. Frigo, S. G. Johnson, "FFTW: an adaptive software architecture for the FFT," *Proceedings of the 1998 IEEE International Conference on Acoustics, Speech and Signal Processing*, vol. 3, 1998, pp. 1381–1384.

[16] B. Bingham, C. Aguero, M. McCarrin, J. Klamo, J. Malia, K. Allen, T. Lum, M. Rawson, R. Waqar, "Toward Maritime Robotic Simulation in Gazebo", *MTS/IEEE OCEANS Conference*, 2019.

[17] M. B. Kramer, J. Andersen, S. Thomas, F. B. Bendixen, H. Bingham, R. Read, N. Holk, E. Ransley, S. Brown, Y. H. Yu, T. T. Tran, J. Davidson, C. Horvath, C. E. Janson, K. Nielsen,m C. Eskilsson, "Highly Accurate Experimental Heave Decay Tests with a Floating Sphere: A Public Benchmark Dataset for Model Validation of Fluid–Structure Interaction", *Energies*, vol. 14, n. 2, 2021.

[18] PX4 Autopilot, Available: https://px4.io/.

[19] S. E. Tavares, "A Comparison of Integration and Low-Pass Filtering", *IEEE Transactions on Instrumentation and Measurement*, Vol. 15, n. 1/2, 1966, pp. 33–38.